Full-Visible-Spectrum Emitters from Pyrolysis of Soluble Si−Si Bonded Network Polymers

Michiya Fujiki,*,† Yoshiki Kawamoto,† Masahiko Kato,† Yuji Fujimoto,† Tomoki Saito,† Shin-ichi Hososhima,† and Giseop Kwak*,‡

Graduate School of Materials Science, Nara Institute of Science and Technology, 8916-5 Takayama, Ikoma, Nara 630-0036, Japan, and Department of Polymer Science, Kyungpook National University, 1370 Sankyuk-dong, Buk-gu, Daegu 702-701, Korea

Received February 26, 2009. Revised Manuscript Received April 15, 2009

Crystalline silicon is a poor UV−visible−near IR emitter because of its indirect, narrow band gap and low quantum yield of $\sim 1 \times 10^{-2}$% at room temperature. To effectively confine a photoexcited electron−hole pair (exciton) within Si's Bohr radius of ~5 nm, we have theoretically and experimentally explored several low-dimensional Si-based materials. Although Si−Si bonded network polysilyne was previously regarded as a soluble model polymer of amorphous Si and Si nanosheet-like "saturated silagraphene," further studies on pyrolytic products of polysilyne derivatives and their inherent photophysical properties under a vacuum have not yet been reported. The present paper demonstrated visible light emission from ten soluble polysilynes in the range 460 nm (2.70 eV) to 740 nm (1.68 eV) at both 77 K and room temperature by controlling temperature and time of the pyrolysis (200−500 °C, 10−90 min) under a vacuum. When very weakly deep-red emitting Si particles produced by the pyrolysis of poly(*n*-butylsilyne) at 500 °C for 90 min were exposed to air, the photoluminescence switched abruptly to an intense sky-blue color ($\lambda = 430$ nm), with a quantum yield of 20−25% and a short lifetime of ~5 ns in common organic solvents at room temperature because of the Siloxene-like, multilayered Si-sheet structures.

Introduction

Crystalline silicon (*c*-Si), the fundamental material for microelectronics, is a poor UV−visible−near IR emitter because of indirect, narrow band gap (1127 nm, 1.1 eV) in low quantum yield (Φ_F) of $\sim 1 \times 10^{-2}$% at 300 K.[1] Since the first reports of fairly efficient photoluminescence (PL) in the visible-near IR region from nanocrystalline Si (*nc*-Si)[2−5] and porous Si,[6,7] much effort has been focused on creating Si with efficient, tunable UV−visible emission. To effectively confine a photoexcited electron−hole pair within Si's Bohr radius of ~5 nm,[1] several low-dimensional Si-based materials have been theoretically[1,8,9] and experimentally explored:[10−36] zero-dimensional *nc*-Si and nanoparticles

* Corresponding author. Fax: 81-743-72-6049 (M.F.); 82-53-950-6623 (G.K.). Tel: 81-743-72-6040 (M.F.); 82-53-9507758 (G.K.). E-mail: fujikim@ms.naist.jp. (M.F.); gkwak@knu.ac.kr (G.K.).
† Nara Institute of Science and Technology.
‡ Kyungpook National University.

(1) (a) Lockwood, D. J. In *Light Emission in Silicon−From Physics to Devices*; Lockwood, D. J., Ed.: Academic: New York, 1998; Chapter 1, pp 1−34. (b) Yu, P. Y.; Cardona, M. *Fundamentals of Semiconductors−Physics and Materials Properties*; 3rd ed.; Springer: New York, 2005; Chapter 7, pp 345−426.
(2) Furukawa, S.; Miyasato, T. *Phys. Rev. B* **1988**, *38*, 5726–5729.
(3) Takagi, H.; Ogawa, H.; Yamazaki, A.; Ishizaki, A.; Nakagiri, T. *Appl. Phys. Lett.* **1990**, *56*, 2379–2381.
(4) (a) Kanemitsu, Y.; Ogawa, T.; Shiraishi, K.; Takeda, K. *Phys. Rev. B* **1993**, *48*, 4883–4886. (b) Kanemitsu, Y. *Phys. Rev. B* **1996**, *53*, 13515–13520. (c) Kanemitsu, Y.; Suzuki, K.; Kyushin, S.; Matsumoto, H. *Phys. Rev. B* **1995**, *51*, 13103–13110.
(5) Wilson, W. L.; Szajowski, P. F.; Brus, L. E. *Science* **1993**, *262*, 1242–1244.
(6) (a) Cullis, A. G.; Canham, L. T. *Nature* **1991**, *353*, 335–338. For a review, see: (b) Cullis, A. G.; Canham, L. T.; Calcott, P. E. J. *J. Appl. Phys.* **1997**, *82*, 909–965.
(7) (a) Lehmann, V.; Gösele, U. *Appl. Phys. Lett.* **1991**, *58*, 856–858. (b) Heitmann, J.; Möller, F.; Zacharias, M.; Gösele, U. *Adv. Mater.* **2005**, *17*, 795–803.
(8) For a review, see: (a) Takeda, K.; Shiraishi, K. *Commun. Condens. Mater. Phys.* **1997**, *18*, 91–133, and references therein. (b) Takeda, K.; Shiraishi, K. *Phys. Rev. B* **1989**, *39*, 11028–11037. (c) Teramae, H.; Takeda, K. *J. Am. Chem. Soc.* **1989**, *111*, 1281–1285. (d) Takeda, K.; Teramae, H.; Matsumoto, N. *J. Am. Chem. Soc.* **1986**, *108*, 8186–8190. (e) Takeda, K.; Shiraishi, K. *Solid State Commun.* **1993**, *85*, 301–305.
(9) For reviews, see: (a) Brus, L. *J. Phys. Chem.* **1994**, *98*, 3575–3581, and references therein. (b) Alivisatos, A. P. *J. Phys. Chem.* **1996**, *100*, 13226–13239, and references therein.
(10) Holmes, J. D.; Ziegler, K. J.; Doty, R. C.; Pell, L. E.; Johnston, K. P.; Korgel, B. A. *J. Am. Chem. Soc.* **2001**, *123*, 3743–3748.
(11) (a) Grom, G. F.; Lockwood, D. J.; McCaffrey, J. P.; Labbe, H. J.; Fauchet, P. M.; White, B., Jr.; Diener, J.; Kovalev, D.; Koch, F.; Tsybeskov, L. *Nature* **2000**, *407*, 358–361. (b) Kovalev, D.; Heckler, H.; Ben-Chorin, M.; Polisski, G.; Schwartzkopff, M.; Koch, F. *Phys. Rev. Lett.* **1998**, *81*, 2803–2806. For a review, see: (c) Kovalev, D.; Fujii, M. *Adv. Mater.* **2005**, *17*, 2531–2544, and references therein.
(12) Gelloz, B.; Kojima, A.; Koshida, N. *Appl. Phys. Lett.* **2005**, *87*, 031107.
(13) Walters, R. J.; Kalkman, J.; Polman, A.; Atwater, H. A.; de Dood, M. J. A. *Phys. Rev. B* **2006**, *73*, 132302.
(14) Jurbergs, D.; Rogojina, E.; Mangolini, L.; Kortshagen, U. *Appl. Phys. Lett.* **2006**, *88*, 233116.
(15) English, D. S.; Pell, L. E.; Yu, Z.; Barbara, P. F.; Korgel, B. A. *Nano Lett.* **2002**, *2*, 681–685.
(16) Fojtik, A.; Henglein, A. *Chem. Phys. Lett.* **1994**, *221*, 363–367.
(17) Li, X.; He, Y.; Swihart, M. T. *Langmuir* **2004**, *20*, 4720–4727.
(18) (a) Liu, S.-M.; Sato, S.; Kimura, K. *Langmuir* **2005**, *21*, 6324–6329. (b) Liu, S.-M.; Yang, Y.; Sato, S.; Kimura, K. *Chem. Mater.* **2006**, *18*, 637–642.
(19) Choi, J.; Wang, N. S.; Reipa, V. *Langmuir* **2007**, *23*, 3388–3394.
(20) For a review, see: Watanabe, A. *J. Organomet. Chem.* **2003**, *685*, 122–133, and references therein.
(21) Pi, X. D.; Liptak, R. W.; Nowak, J. D.; Wells, N. P.; Carter, C. B.; Campbell, S. A.; Kortshage, U. *Nanotechnology* **2008**, *19*, 245603.
(22) For a review, see: Liu, S.-M. *J. Nanosci. Nanotechnol* **2008**, *8*, 1110–1125, and references therein.

10.1021/cm900567g CCC: $40.75
Published on Web 05/12/2009

Scheme 1. General Synthetic Scheme and Photograph of *n*-BSNP in Chloroform

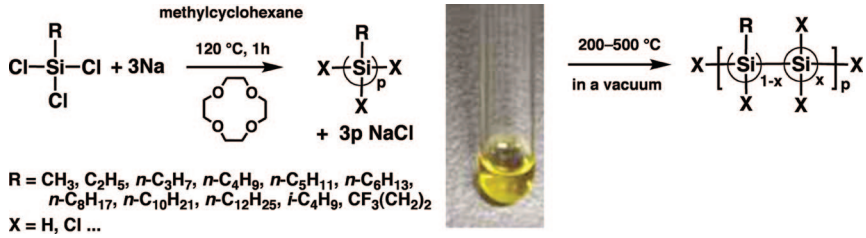

as visible−near IR emitters,[10−26] Si nanowire[27,28] and one-dimensional helical polysilane as an exitonic UV emitter[29] and a two-dimensional (2D) skeleton as a visible emitter, such as Si−Si bonded network polysilyne (SNP),[8,30−32,36] Wöhler Siloxene,[33] and Si/SiO_2 superlattice.[35] Although SNP was previously regarded as a soluble model polymer of amorphous Si (*a*-Si)[36] and 2D-Si nanosheet-like "saturated bonded sila-graphene",[4,8a,b,33,34] further studies[30] on pyrolytic products of SNP derivatives and their inherent photophysical properties under a vacuum and low temperature have not yet been reported. Here we report visible-light emission from 10 soluble SNPs (Scheme 1 and Figure S1 in the Supporting Information) in the range 460 nm (2.70 eV) to 740 nm (1.68 eV) at both 77 K and room temperature by controlling the temperature and time of the pyrolysis (200−500 °C, 10−90 min) under a vacuum. When very weakly deep-red emitting Si particles produced by the pyrolysis of poly(*n*-butylsilyne) (*n*-BSNP) at 500 °C for 90 min were exposed to air, the PL switched abruptly to an intense sky-blue color ($\lambda = 430$ nm) with a Φ_F of 20−25% and a short lifetime of ∼5 ns dispersed in common organic solvents at room temperature because of the Siloxene-like, multilayered Si-sheet structures.

Results and Discussion

Revisited Pyrolysis Study of Polysilyne. Pyrolysis of Si-containing polymers, including poly(dimethylsilane),[37] polycarbosilane (PCS),[38,39] and chlorine containing polysilane,[40] has long been known to produce exclusively β-silicon carbide (SiC). This led to the idea that SNP may also produce β-SiC. However, thermogravimetric (TG) and isothermal thermogravimetric (ITG) analyses of the 10 SNPs studied in this work in a stream of pure nitrogen gas (99.99%) indicate production of elemental Si. The TG data (Figure 1) show that SNPs underwent degradation in two steps: except for sterically crowded isobutyl (*i*-BSNP) and trifluoropropyl (FPSNP) derivatives, most SNPs began to degrade at ∼300 °C, implying elimination of an alkylene moiety[37−41] because of a β-H shift from the alkyl side group to the Si skeleton, followed by the release of hydrogen gas from the Si−H bond at ∼450 °C. Both *i*-BSNP and FPSNP derivatives began to degrade at temperatures as low as ∼250 °C (all SNP data and pyrolysis schemes are shown in Figure S2 in the Supporting Information). ITG data of SNPs at 500 °C as a function of pyrolysis time (Figure 2) suggested that the observed weight loss of SNP after prolonged (90 min) pyrolysis correspondings to a residue of pure Si (not SiC), regardless of alkyl side group (Figure 3).

This was further proved by scanning electron microscopy (SEM)/X-ray photoelectron spectroscopy (XPS)/energy dispersive X-ray spectroscopy (EDS) analysis of the 900 °C pyrolysis product of *n*-propyl-SNP and *n*-BSNP, which showed that the surface is probably oxidized, as evidenced by 1:1 signals of Si and O, but no C signal due to SiC (Figures S3 and S4 in the Supporting Information). As postulated in PCS pyrolysis experiments,[38,39] β-H elimination from alkyl C−H (see Scheme S1 in the Supporting Information) may play a key role in the production of Si without significant occurrence of the Kumada rearrangement reaction responsible for SiC formation.[41] Peripheral structures of SNPs may be terminated with Si−Cl and Si−H, as exmplified in chlorine containing polysilane.[40] For most SNPs, Si−Cl and Si−H bonds were evident from broad ^{29}Si-FT-NMR signals at ∼30 ppm and from the broad FT-IR signal around 2080

(23) (a) Bley, R. A.; Kauzlarich, S. M. *J. Am. Chem. Soc.* **1996**, *118*, 12461–12462. (b) Mayeri, D.; Phillips, B. L.; Augustine, M. P.; Kauzlarich, S. M. *Chem. Mater.* **2001**, *13*, 765–770. (c) Zou, J.; Baldwin, R. K.; Pettigrew, K. A.; Kauzlarich, S. M. *Nano Lett.* **2004**, *4*, 1181–1186. (d) Zhang, X.; Brynda, M.; Britt, R. D.; Carroll, E. C.; Larsen, D. S.; Louie, A. Y.; Kauzlarich, S. M. *J. Am. Chem. Soc.* **2007**, *129*, 10668–10669.
(24) Wilcoxon, J. P.; Samara, G. A.; Provencio, P. N. *Phys. Rev. B* **1999**, *60*, 2704–2714.
(25) (a) Hua, F.; Erogbogbo, F.; Swihart, M. T.; Ruckenstein, E. *Langmuir* **2006**, *22*, 4363–4370. (b) Hua, F.; Swihart, M. T.; Ruckenstein, E. *Langmuir* **2006**, *22*, 6054–6062.
(26) Nayfeh, M.; Mitas, L. In *Nanosilicon*; Kumar, V. Ed.; Elsevier: Oxford, U.K., 2008; Chapter 1, pp 1−78.
(27) Qi, J.; Belcher, A. M.; White, J. M. *Appl. Phys. Lett.* **2003**, *82*, 2616–2618.
(28) Ma, D. D. D.; Lea, S. T.; Shinar, J. *Appl. Phys. Lett.* **2005**, *87*, 033107.
(29) (a) Fujiki, M. *Macromol. Rapid Commun.* **2001**, *22*, 539–563. (b) Fujiki, M. *Appl. Phys. Lett.* **1994**, *65*, 3251–3253. (c) Fujiki, M. *J. Am. Chem. Soc.* **1994**, *116*, 6017–6018. (d) Hasegawa, T.; Iwasa, Y.; Koda, T.; Kishida, H.; Tokura, Y.; Wada, S.; Tashiro, H.; Tachibana, H.; Matsumoto, M. *Phys. Rev. B* **1996**, *54*, 11365–11374.
(30) (a) Bianconi, P. A.; Schilling, F. C.; Weidman, T. W. *Macromolecules* **1989**, *22*, 1697–1704. (b) Bianconi, P. A.; Weidman, T. W. *J. Am. Chem. Soc.* **1988**, *110*, 2342–2344.
(31) Smith, D. A.; Joray, S. J.; Bianconi, P. A. *J. Polym. Res.* **2005**, *12*, 393–401.
(32) Furukawa, K.; Fujino, M.; Matsumoto, N. *Macromolecules* **1990**, *23*, 3423–3426.
(33) Brandt, M. S.; Vogg, G.; Stutzmann, M. In *Silicon Chemistry*; Jutzi, P.; Schubert, U., Eds.; Wiley-VCH: Weinheim, Germany, 2003; Chapter 15, pp 194−213.
(34) Nesper, R. In *Silicon Chemistry*; Jutzi, P., Schubert, U., Eds.; Wiley-VCH: Weinheim, Germany, 2003; Chapter 13, pp 171−180.
(35) Lu, Z. H.; Lockwood, D. J.; Baribeau, J.-M. *Nature* **1995**, *378*, 258–260.
(36) Wilson, W. L.; Weidman, T. W. *J. Phys. Chem.* **1991**, *95*, 4568–4572.
(37) (a) Yajima, S.; Hasegawa, Y.; Hayashi, J.; Okamura, K. *J. Mater. Sci.* **1978**, *13*, 2569–2576. (b) Yajima, S.; Hayashi, J.; Omori, M.; Okamura, K. *Nature* **1976**, *261*, 683–685. (c) Yajima, S.; Hayashi, J.; Omori, M. *Chem. Lett.* **1975**, 931–934.
(38) Liu, Q.; Wu, H.-J.; Lewis, R.; Maciel, G. E.; Interrante, L. V. *Chem. Mater.* **1999**, *11*, 2038–2048.
(39) Schmidt, W. R.; Interrante, L. V.; Doremus, R. H.; Trout, T. K.; Marchetti, P. S.; Maciels, G. E. *Chem. Mater.* **1991**, *13*, 257–267.
(40) Martin, H.-P.; Müller, E.; Richter, R.; Roewer, G.; Brendler, E. *J. Mater. Sci.* **1997**, *32*, 1381–1387.
(41) Shini, K.; Kumada, M. *J. Org. Chem.* **1958**, *23*, 139–139.

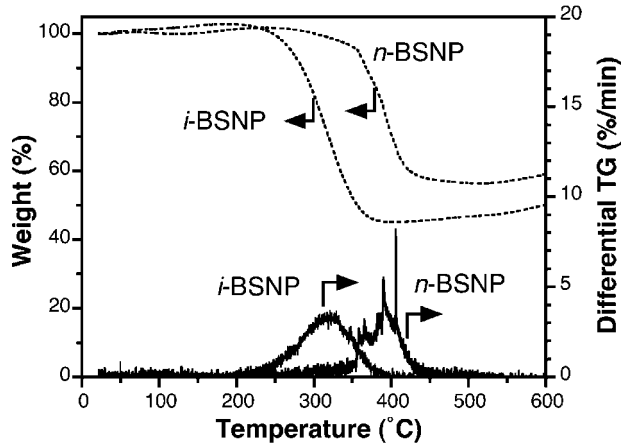

Figure 1. Thermogravimetric (TG) and differential TG charts of *n*-BSNP and *i*-BSNP in a N_2 atmosphere with heating rate of 5 °C min^{-1}.

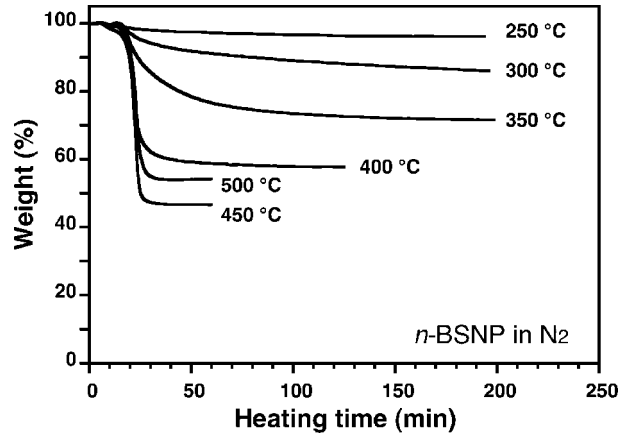

Figure 2. ITG charts of *n*-BSNP in a stream of N_2 gas at given temperatures (250, 300, 350, 400, 450, 500 °C). ITG curves between 450 and 500 °C appeared to be reversed. This was reproducible and probably due to rapid evolution of some volatile sources from *n*-BSNP during a prolonged heating at 450 °C.

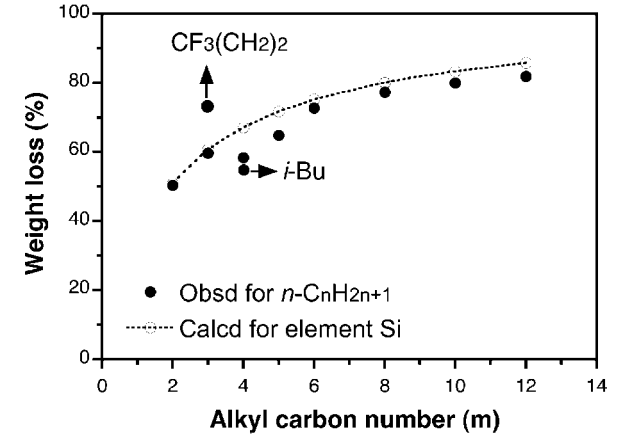

Figure 3. Weight loss of ten SNPs with different alkyl chains pyrolyzed at 500 °C for 90 min. Filled and open circles with dotted line are experimental and calculated values for elemental Si, respectively.

cm^{-1}, respectively (Figures S5−S8 in the Supporting Information). The free Cl atom from the Si−Cl bond may catalyze efficient β-H elimination. This unexpected result may be a common feature for Si−Si bonded molecules and polymers bearing appropriate side groups in an oxygen-free environment. Indeed, an Si−Si bonded cubic molecule with bulky

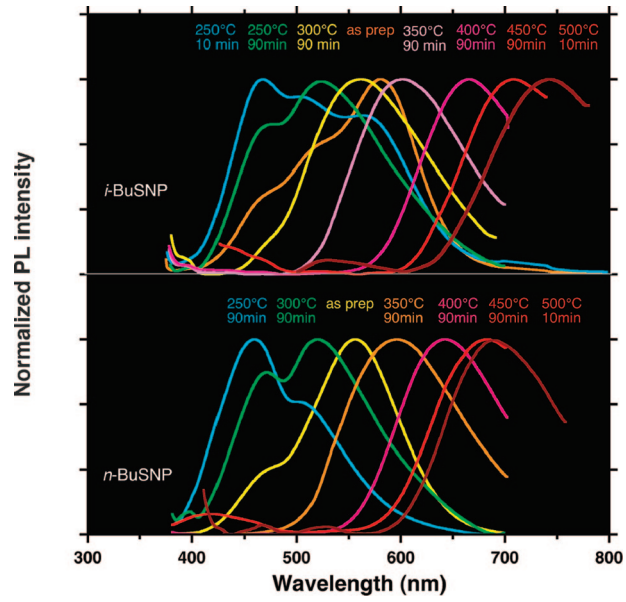

Figure 4. Changes in the optical spectra of *n*-BSNP and *i*-BSNP film during pyrolysis: PL spectra of *n*-BSNP (bottom) and *i*-BSNP (top) films excited at 360 nm at 77 K at different pyrolysis temperatures for 10 and 90 min.

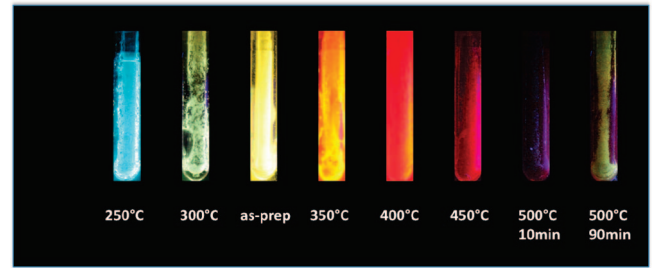

Figure 5. Photographs of *n*-BSNP film with different pyrolysis conditions.

organic groups, octa(*tert*-butyl)octasilacubane was transformed into an *a*-Si film by pyrolysis in a vacuum at 350−450 °C.[42] Polycrystalline Si thin film with a high-carrier mobility was made by pyrolysis of Si−Si bonded linear polymer, $(SiH_2)_n$, at 300−550 °C in an oxygen-free glovebox.[43]

Changes in Photoluminescence and Photoluminescence Excitaion Spectra of Polysilyne by Vacuum Pyrolysis. Figure 4 shows the change in the PL spectra of *n*-BSNP and *i*-BSNP films excited at 360 nm at 77 K that were treated at several different pyrolysis temperatures for 10 and 90 min. For clarity, Figure 5 displays several photographs of these *n*-BSNP films. Before the pyrolysis, the *n*-BSNP virgin film emitted a yellowish PL band peaking at 560 nm with two fast lifetime components of 1.3 and 5.8 ns. When the film was treated at 250 °C for 90 min, the PL band was markedly blue-shifted and showed a blue PL band at 460 nm. When the virgin films were treated at 300 °C for 90 min, the PL band was shifted slightly to green at 520

(42) Furukawa, K. Synthesis and Optical Properties of Silicon-Backbone Materials: $(RSi)_n$ (R = Organic Group). Ph.D. Thesis, Waseda University, Tokyo, 2000; Chapter 7 (in Japanese).
(43) Shimoda, T.; Matsuki, Y.; Furusawa, M.; Aoki, T.; Yudasaka, I.; Tanaka, H.; Iwasawa, H.; Wang, D.; Miyasaka, M.; Takeuchi, Y. *Nature* **2006**, *440*, 783–786.

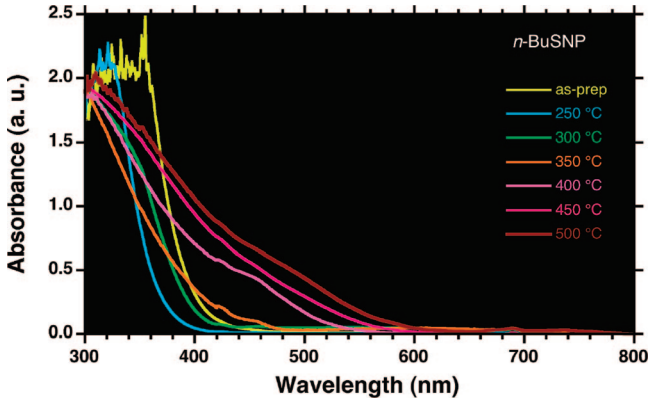

Figure 6. UV−vis absorption spectra (normalized at 300 nm) of *n*-BSNP films after pyrolysis at different temperatures for 10 and 90 min.

nm. On the other hand, when the virgin films were treated at 350, 400, and 450 °C for 90 min, the PL wavelength from the film emission progressively red-shifted: for 350 °C, orange at 580 nm; for 400 °C, red at 640 nm; for 450 °C, deep-red at 680 nm. Similarly, the *i*-BSNP film progressively shifted first toward blue and then toward red. When the virgin *i*-BSNP film was treated at 500 °C for 10 min, it attained the deepest red PL as long as 740 nm. Both *n*-BSNP and *i*-BSNP treated at 250−300 °C for 90 min showed greenish white emission by the naked eye (Figure 5), as expected from the spectral profiles in Figure 4.

When the *n*-BSNP virgin film was treated at 500 °C for 90 min, it became a metallic lustrous film, emitting very weak, deep-red PL around 680 nm with a marked decrease in intensity: one-sixth that of the sample treated at 500 °C for 10 min (Figures 4 and 5). Figure 6 shows these marked progressive blue- and red-shifts in the UV−visible absorption edge of the pyrolyzed SNP films kept in sealed tubes with increasing pyrolysis temperature. This change in UV−vis absorption edge corresponds well with the change in blue- and red-shifts of the PL bands. It is noteworthy that the SNP film treated at 500 °C clearly showed broad absorption bands in the range of 350−600 nm, indicating a significant change in Si−Si bonded skeleton.

Although exact Φ_F values of these films were not determined, they were assumed to be several % (not exceeding 10%) at 77 K, based on the fact that the PL intensity of the films at room temperature was one-sixth that at 77 K (see Figure S9 in the Supporting Information) and that the Φ_F value from virgin *n*-BSNP in THF solution at room temperature was ∼1% with reference to 9,10-diphenylanthracene ($\Phi_F \sim 97\%$ in methylcyclohexane, see Figure S11 in the Supporting Information). For the virgin film at 300 °C, the PL band at 560 nm at 77 K excited at 370 nm had fast and slow lifetime components of ∼5 ns and >10 ns. This short lifetime should be compared to the long one of intrinsic *c*-Si of 4.6 h.[40] The oxygen may be inserted into the SNP skeleton, as the SNP film was sealed in the presence of a small amount of air (∼3×10^{-1} Torr). Indeed, a film prepared in a trace amount of air (∼5×10^{-5} Torr) showed that the major PL band around 550 nm was almost unchanged, even after thermal treatment at 200 and 300 °C (see Figure S10 in the Supporting Information). Controlling the time and temperature of the air-oxidation and pyrolysis

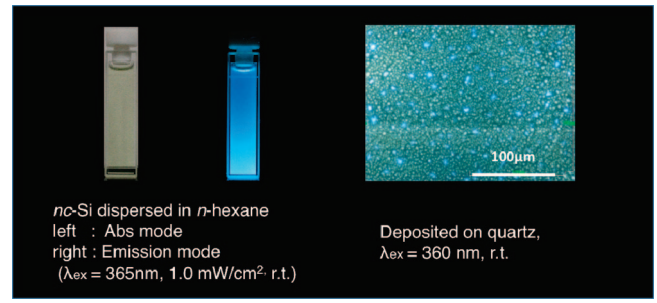

Figure 7. Photographs of air-exposed *nc*-like-Si particles prepared from *n*-BSNP (500 °C, 90 min).

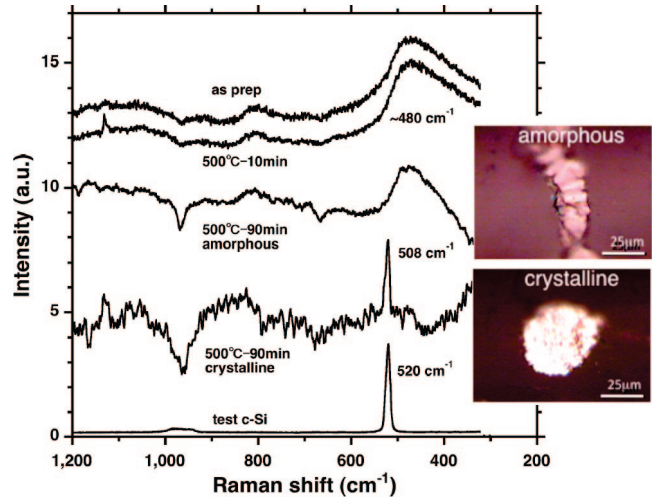

Figure 8. Laser Raman spectra and microscope images of *n*-BSNP pyrolysis products prepared at 500 °C for 10 and 90 min and virgin *n*-BSNP film.

of the virgin SNP film may thus facilitate tuning of the PL wavelength from 460 nm (2.70 eV) to 740 nm (1.66 eV).

When the Si particles emitting very weak deep-red light under 360 nm excitation in solution and on a solid substrate were exposed to air at room temperature, they immediately emitted sky-blue light at 430 nm (2.88 eV) (Figures 4 and 7). The particles were produced by pyrolysis at 500 °C for 90 min, followed by filtering with a membrane (0.1 μm pore) to remove the α-Si portion. The Φ_F value obtained from the air-oxidized Si particles excited at 360 nm was dependent on the solvent used in the dispersion at room temperature (Figure 7 and Figure S11 in the Supporting Information): 25% in dimethylformamide, 23% in methanol, 20% in tetrahydrofuran, 19% in chloroform, 16% in toluene, 15% in acetone, 15% in *n*-hexane, and only 1% in water. Although the Φ_F values tend to increase as solvent polarity increases, the particles may be water-sensitive, leading to nonemissive particles because of the loss of organic protecting groups at the particle surface. In *n*-hexane, the particles at 560−640 nm had two lifetime components of ∼4.2 ns and >10 ns (see Figure S12 in the Supporting Information).

UV−Visible, Photoluminescence, Photoluminescence Excitaion, and Raman Spectra of Pyrolitic Product of Polysilyne. Figure 8 compares laser Raman microscope analyses of the *n*-BSNP pyrolysis products at 500 °C for 10 and 90 min with Raman spectra of the virgin *n*-BSNP film. These suggest the coexistence of several particles with ∼30 μm size: regions with a metallic luster had a sharp Raman

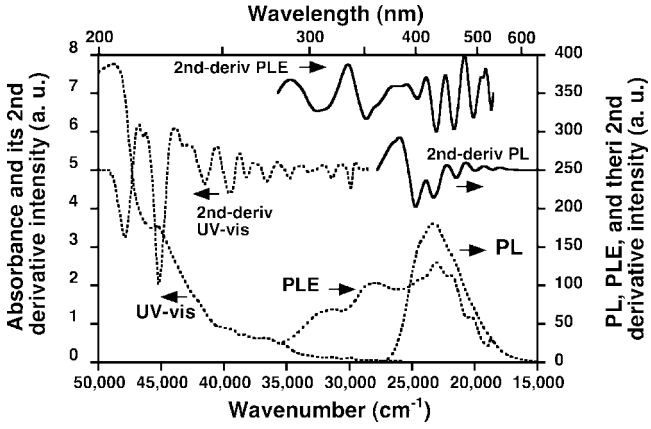

Figure 9. PL (excited at 360 nm), PL excitation (PLE, monitored at 540 nm), and UV−vis absorption spectra with their second derivative spectra of the air-exposed *nc*-like-Si particles dispersed in *n*-hexane.

resonance at 508 cm^{-1}, probably due to *nc*-like-Si particles, and nonmetallic luster regions (amorphous regions) had a very broad Raman shift at ∼460 cm^{-1}, as for the virgin *n*-BSNP film.

Figure 9 shows PL (excited at 360 nm), PL excitation (PLE, monitored at 540 nm), and UV−vis absorption spectra with their second derivative spectra of the air-exposed Si particles dispersed in *n*-hexane. As evident from the second derivative spectra, these apparent broad PL, PLE, and absorption spectra consist of at least five well-resolved bands and several additional bands with almost equal energy spacing: 1650 ± 100 cm^{-1} from UV−vis, 1580 ± 200 cm^{-1} from UV−vis, 1470 ± 70 cm^{-1} from PLE.

This oscillating behavior may be related to the combination of bands due to the Si−Si stretching mode of the 2D-like Si skeleton located at ∼460 cm^{-1} and the Si−O−Si stretching mode at ∼1100 cm^{-1}. An efficient coupling between electron (due to the Si−Si skeleton) and phonon (due to Si−O−Si stretching vibration) might be responsible for such a strongly blue emissive mode due to the loss of translational symmetry. Indeed, if the plural electronic transitions in the PL, PLE, and UV−vis spectra came from purely electronic origins with 2D structure, the energy separation (E_n) should obey the inverse of square of the quantum number, *n* (eq 1). If the transitions were connected to vibronic transitions, the separation will simply be related to *n* in a parabolic potential well (eq 2). The air-exposed *nc*-like-Si particle is presumably an example of the latter case, while the unexposed *nc*-like-Si samples may be of the former type due to very weak electron−phonon coupling.[1b,44,45]

$$E_n = \hbar^2/2m(\pi/na)^2, \text{ purely electronic transitions with } n \quad (1)$$

$$E_n = (n + 1/2)\hbar\omega, \text{ purely vibronic transitions with } n \quad (2)$$

High-resolution transmission electron microscopy (HRTEM) with EDS, fluorescence optical microscopy (FOM), atomic force microscopy (AFM) and wide-angle X-ray diffraction (WAXD) photographs of the air-exposed Si particles, along with Raman/IR spectra, may allow for the determination of the origin of the blue- and red-emissive structures in the pyrolysis products.

Microscopic Images of Pyrolitic Product of Polysilyne. Figure 10 depicts two HRTEM images of the air-exposed Si particles. Because of mechanical shaking during the sample filtration step, the major portions (highly magnified images, Figure S13 in the Supporting Information) showed very fine *nc*-Si particles ∼1 nm in diameter with a lattice spacing of ∼0.25 nm, as well as the existence of oxygen in the portions with a ratio of Si/O ≈ 1/3 by EDS analysis. However, because of incomplete mechanical shaking, the two HRTEM images clearly show "baum-küchen-like," multilayered structures (magnified images, Figures S14 and S15 in the Supporting Information): Figure 10 (left) shows circular shapes with ∼0.34 nm spacing; Figure 10 (right) shows lamellar shapes with ∼0.37 nm spacing. WAXD images of *n*-BSNP and pyrolyzed *n*-BSNP indicated that the former has a *d*-spacing of 0.55 nm ($2\theta \approx 16°$, CuK_a), implying an interlayer spacing between *n*-BSNP multisheets, whereas the latter has no such ordered structures (Figure S16 in the Supporting Information). These layered structures imply that the air-exposed Si particles are 2D-Wöhler-Siloxene[33] separated by a highly stretched Si−O−Si bond with an opened Si−O−Si bond angle (Figure 11). The origin of the blue-shifted PL band at 250 °C is thus assumed to be due to the partial oxidation of the SNP single-sheet, when oxygen gas in the closed tube is consumed during the pyrolysis. AFM images of the particles deposited on mica suggested several sizes of flat ring disk shapes, ranging from 1.5 to 10 nm in height and from 0.5 to 1 μm in diameter (Figure S17 in the Supporting Information).

An almost oxygen-free sealed condition showed no such blue-shift PL when operated at 200−300 °C. The origin of the progressively red-shifted PL band at more elevated temperatures is conjectured to be multilayer structures formed by the spontaneous stacking of 2D-SNP single-sheets due to the elimination of the organic moieties and hydrogen during pyrolysis. The PL wavelength is tunable via the thickness of the Si film.[35] Assuming an Si−Si bond length projected in the stacking direction of 0.185 nm, the Si layer number extrapolated from the PL peak wavelength can be calculated by the simple equation[35] given for the Si/SiO_2 superlattice of E_{PL} (eV) = 1.6 + 0.7/d_{Si}^2.

Figure 12 plots the PL energy in eV as a function of estimated thickness and number of layers. Macroscopically curved cracked structures were evident from optical microscope (OM) images of the *n*-BSNP and *i*-BSNP samples at 350−500 °C (Figure S18 in the Supporting Informatino). When the pyrolyzed SNP without any organic or H moieties was exposed to air, a spontaneous insertion of oxygen atoms into the multilayer Si ultrathin films occurred, resulting in the formation of a periodic $(Si)_1/(SiO_2)_1$ superlattice[35] identical to the Wöhler−Siloxene multilayers[33] with Si−O−Si interspacing. The theory previously predicted in 1993 that a Wöhler−Siloxene bearing oxygen moieties could be highly emissive due to change from the indirect- to direct-type band

(44) Konagai, M. *The Handotai Chokoshi Nyumon (Introduction to Semiconductor Superlattice)*; Baifukan: Tokyo, 1987 (in Japanese).
(45) Davies, J. H. *The Physics of Low-Dimensional Semiconductors: An Introduction*; Cambridge University Press: Cambridge, U.K., 1998.

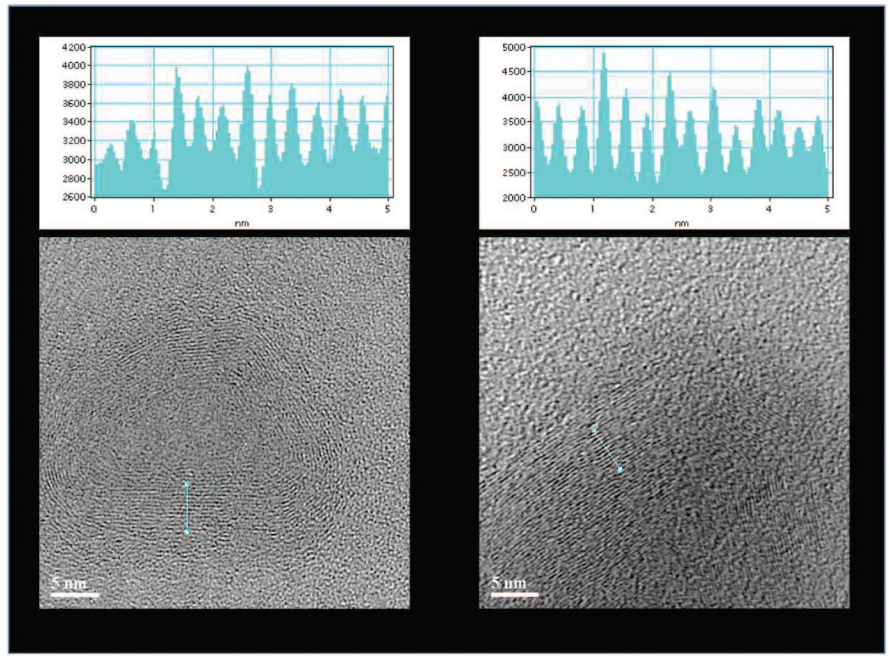

Figure 10. HRTEM images of the air-exposed *nc*-Si particles with multilayered structures (left, circular shapes with ~0.34 nm spacing; right, lamellar shapes with ~0.37 nm spacing).

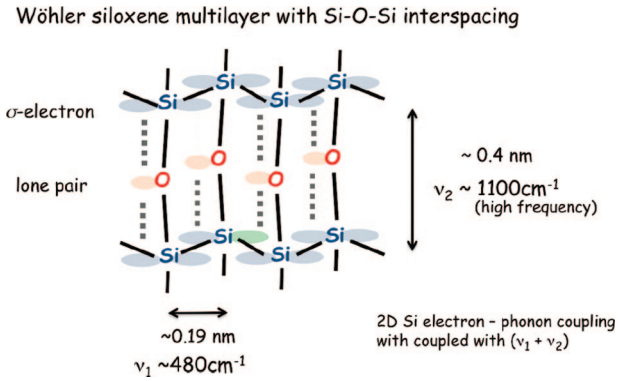

Figure 11. Proposed layered structures of the air-exposed Si particles which are similar to 2D-Wöhler−Siloxene[33] separated by a highly stretched Si−O−Si bond with an opened Si−O−Si bond angle.

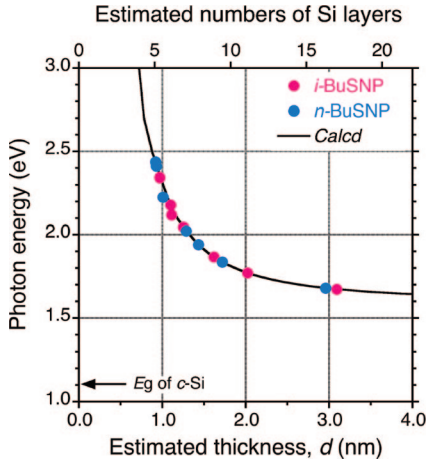

Figure 12. Estimated numbers of Si multilayers extrapolated from the PL peak energy of *n*-BSNP and *i*-BSNP based on the simple equation (E_{PL} (eV) = 1.6 + 0.7/d_{Si}^2) for a Si/SiO_2 superlattice.[35]

structures.[4,8] This change results from characteristic σ-*n* orbital mixing of the 2D-Si σ electrons with oxygen's lone pair electrons at the band-edge states for an ideal 2D-Si polymer bearing OH and H side groups.[8e]

Proposed Scheme from Soluble Organopolysilyne to Insoluble Wöhler−Siloxene-like Structure by Vacuum Pyrolysis. Finally, Figure 13 schematically proposes a change in structural hierarchy based on a model of Wöhler−Siloxene multisheet separated by an Si−O−Si linkage at elevated pyrolysis temperatures, followed by exposure to air. The soluble PNSs and their pyrolysis products, due to easy coating and dispersion in the form of Si-ink, in comparison to a series of II−VI group nanocrystals,[9b,46] have the benefit of being Si-source materials serving as full-visible-spectrum emitters at room temperature (see Figure S19 in the Supporting Information). The ionization potential and electron affinity of the pyrolyzed Si materials range between 5.2 and 5.4 eV and 4.0 and 3.2 eV, respectively,[35] enabling an easy match with the work-functions of ITO and Al/Ag/Mg electrodes. Recently, air-stable red-green-blue *nc*-Si emitters were achieved by the use of SiH_4 plasma following CF_4 plasma etching.[21] Our controlled vacuum pyrolysis using a single SNP source material may thus lead to a new environmentally friendly, safer process to produce red-green-blue Si emitters, since the required technology is mostly compatible with XeCl excimer laser annealing and the crystallization process of making *poly*-Si TFT from *a*-Si thin film deposited by the SiH_4−Si_2H_6 CVD process. Additionally, the present result could lead to better understanding of intrinsic nature on pseudo-2D Si electronic structure by varying Si layer numbers, that are influenced by a trace amount of oxygen (air).

(46) Colvin, V. L.; Schlamp, M. C.; Alivisatos, A. P. *Nature* **1994**, *370*, 354–357.

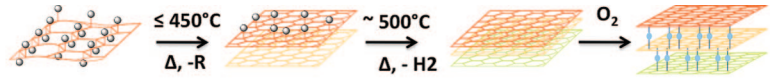

Raman shift /cm^{-1}	~ 460	~ 460	508	~480
Estimated Si layers	1	3–7	> 8–15	1 with Si-O-Si
Band gap Eg /eV	2.1	1.8 – 2.7	~ 1.1 ?	2.9

Figure 13. Proposed scheme of changes in the structural hierarchy of SNP from 2D single-sheet to quasi-3D multisheet, based on optical gap of SNPs or pyrolysis followed by exposure to air. The model is based on a Wöhler−Siloxene-like structure with and without Si−O−Si interlayer spacers.

Experimental Section

Synthesis of SNPs. All soluble SNPs were synthesized by sodium-mediated reduction of the corresponding alkyltrichlorosilanes (Shin-Etsu and Gelest) in the presence of a crown ether cocatalyst under a N_2 atmosphere. All trichlorosilanes were distilled prior to use. To prevent any contact of the SNP with air and moisture during all procedures, including preparation, isolation, and sample sealing in a glass tube, we typically synthesized *n*-BSNP in the following manner, as shown in Scheme 1. Methylcyclohexane (TCI, dried over 4A molecular sieves or CaH_2, 4 mL) containing Na (Wako, 0.43 g, 19 mmol) and 12-crown-4-ether (Aldrich, 0.02 g, 0.11 mmol) was placed in a four-necked 100 mL flask and refluxed at 120 °C with mechanical stirring. To this mixture was added dropwise *n*-butyltrichlorosilane (Shin-Etsu, 0.98 g, 5.1 mmol) dissolved in methylcyclohexane (4 mL). After the addition was completed, the reaction mixture was stirred for 1 h and allowed to cool to room temperature. The reaction vessel was moved to a glovebox filled with 99.9% N_2 gas.

A clear yellow solution containing SNP (see Scheme S1 in the Supporting Information) was obtained by a pressured filtration of the reaction mixture using a fluorinated membrane filter (Advantec, Labodisc, 0.50 mm pore) to remove excess Na and NaCl. The polymer was isolated by precipitating the solution in dry acetone (Aldrich) and dried in the box by connecting to an external vacuum pump outside. No IR spectroscopic evidence of the Si−O−Si vibration at 1000−1100 cm^{-1} in the fresh SNP was obtained. Similarly, ethyl, *n*-propyl, *i*-butyl, *n*-pentyl, *n*-hexyl, *n*-octyl, *n*-decyl. *n*-dodecyl, and 3,3,3-trifluoropropyl derivatives were also prepared. Soluble methyl SNP was not isolated due to its extreme insolubility. Weight-average and number-average molecular weights (M_w and M_n) of isolated SNPs are given in Figure S1 and Table S1 in the Supporting Information. The isolated yield of SNP was typically 40−50% when the crude SNP was precipitated into methanol outside the glovebox with no precaution taken against air/moisture. This value was almost identical to a previous report.[32] Because this workup process was done in a glovebox, not all yields were determined, in order to avoid any contact with contaminants during the weighing of samples.

Preparation of SNP Film and Pyrolysis in a Tube. A methylcyclohexane solution of SNP was placed into a glass tube (ID 5 mm, OD 7 mm), followed by manual coating of the tube inner wall and drying by blowing with N_2 gas. The SNP film deposited in a glass tube was connected to a two-way vacuum bulb. The glass tube coated with the SNP film was removed from the glovebox and sealed by a hand-burner using vacuum techniques (0.3 Torr by rotary pump or 5×10^{-5} Torr by a Pfeiffer turbo molecular pump). In pyrolysis experiments and PL/PLE measurements, the glass tube was placed into a housing made of an aluminum block and onto a digitally controlled hot plate (Thermolyne), and the temperature of the housing was monitored with a chromel-alumel thermocouple (see Scheme S1 in the Supporting Information).

Characterization and Measurements. The M_n and M_w values were evaluated by size exclusion chromatography with a UV−vis photodiode array detector at 40 °C based on a calibration by polystyrene standards on a Shimadzu A10 instrument, performed using PLgel 10 μm mixed-B (Polymer Laboratories) as a column and tetrahydrofuran (THF) as eluent. UV−vis absorption spectra were recorded on a JASCO V-570 spectrophotometer (bandwidth 2 nm). PL and PLE spectra were measured using a JASCO FP-6500 spectrofluorometer equipped with a housing immersed in liquid N_2 designed for phosphorescence measurement (bandwidths 2 nm for excitation and emission). FT-NMR (^{1}H and ^{29}Si{^{1}H}) spectra were measured in $CDCl_3$ (Merck and Aldrich) with a JEOL JNM-LA400 FT-NMR spectrometer using tetramethylsilane as an internal standard. FT-IR spectra were obtained on a Horiba FT-730 spectrometer by casting a solution of SNP onto a KBr substrate in a N_2 atmosphere. Laser Raman microscope images and spectra were obtained on a JASCO NRS-210 (Ar CW-laser 514.5 nm, 10 mW) using the backscattering mode. SNPs sealed in a tube and/or placed onto an Au-coated plate in N_2 atmosphere were measured. TG and ITG measurements were performed in a stream of N_2 gas (5 °C/min for heating) using a MAC Science TG-DTA-2000S and a Seiko Exstar 6200 TG-DTA. CCD images were recorded on a Nikon Eclipse E400 fluorescence microscope equipped with a Nikon DL-5 M digital camera. Optical microscopic photographs were taken with an Olympus BX50 polarizing optical microscope equipped with an Olympus CCD camera. HRTEM images were obtained with a JEOL JEM-3100FEF electron microscope (300 kV, bright image) and EDS with a JEOL EM-Z01299TJEC. Samples for HRTEM were prepared by casting an *n*-hexane solution on an elastic carbon film-coated microgrid (Oken-Shoji). Tapping-mode AFM imaging was conducted under ambient conditions on a Veeco Nanoscope III with multimode. A THF solution of SNPs was deposited on fresh mica. XPS analysis was conducted on a Kratos Axis 165 (Al-K_α, 10 mA, 15 kV). SEM imaging was operated on a JEOL JSM-6301F. WAXD data were used on a Rigaku R-AXIS wide-angle X-ray diffractometer (45 kV, 50 mW) and analyzed by Rigaku automatic X-ray imaging software.

Conclusions

Although *c*-Si is the most archetypal semiconducting materials for microelectronics, it is a poor visible emitter with a quantum yield of 0.01% at 300 K and long PL lifetime of several hours. Although pyrolysis of chain-like Si-containing polysilane and polycarbosilane has already been shown to efficiently produce SiC, our TG and ITG pyrolysis experimental results on various soluble SNPs indicated production of elemental Si. It was found that SNP become a visible emitter tunable from 460 nm (2.7 eV) to 740 nm (1.68 eV) at both 77 K and room temperature by controlling pyrolysis temperature and time (200−500 °C, 10−90 min). Moreover, air-exposed *nc*-like-Si, produced by pyrolyzing SNP at 500 °C, showed an intense blue PL peaking at 430 nm with a quantum yield of 20−25% and a short lifetime of ~5 ns dispersed in common organic solvents at room temperature. HR-TEM, laser-Raman, and second-derivative

UV−vis, PL, and PLE spectra indicated that the Siloxene-like, multilayered Si-sheet structures are responsible for a wide range of visible PL color with a high quantum yield. The chemistry of vacuum thermolysis of SNP, which is available by a sodium-mediated condensation of the corresponding organotrichlorosilane in organic solvent, may thus open a new way to safely produce silicon-based luminescent materials (blue, green, red, and infrared) and nonluminescent elemental silicon.

Acknowledgment. This work was supported by a Grant-in-Aid for Science Research in a Priority Area "Super-Hierarchical Structures (17067012)" from the Ministry of Education, Culture, Sports, Science and Technology, Japan (FY2005−2008) and was supported by a Nippon Sheet Glass Foundation for Materials Science and Engineering (FY2009). The authors thank Kyozaburo Takeda, Kenji Shiraishi, Nobuo Matsumoto, Masaie Fujino, Akira Watanabe, Masanobu Naito, Kotohiro Nomura, Akiharu Satake, Kazuaki Furukawa, Masaaki Ishikawa, Anubhav Saxena, Takuma Kawabe, and Hisanari Onouchi, for their stimulating discussion and contribution to the present preliminary work. M.F. thanks Julian R. Koe at International Christian University (Tokyo) for helpful discussion and for critical reading of the entire text in its original form.

Supporting Information Available: GPC, TG, SEM, EDS, FT-IR, ^{29}Si NMR, PL, PL lifetime, HRTEM, WAXD, AFM, optical microscopy (OM), and fluorescent optical microscopy (FOM) of materials studied in this work (PDF). This material is available free of charge via the Internet at http://pubs.acs.org.

CM900567G